

Magnetic diffusion driven shear instability of solar flux tubes

B.P. Pandey and Mark Wardle

*Department of Physics, Astronomy & Research Centre for Astronomy, Astrophysics & Astrophotonics,
Macquarie University, Sydney, NSW 2109, Australia*

1 August 2012

ABSTRACT

The dynamics of the partially ionised solar photosphere–chromosphere can be described by a set of equations that are structurally similar to the magnetohydrodynamic equations, except now the magnetic field is no longer *frozen* in the fluid but slips through it due to non-ideal magnetohydrodynamic effects which manifests itself as Ohm, ambipolar and Hall diffusion. Macroscopic motion of the gas is widespread throughout the solar atmosphere and shearing motions couple to the non-ideal effects, altogether destabilising low frequency fluctuations in the medium. The origin of such non-ideal magnetohydrodynamic instability lies in the collisional coupling of the neutral particles to the magnetized plasma in the presence of sheared background flows. Expectedly the maximum growth rate and most unstable wavenumber depend on the flow gradient and ambient diffusivities.

The orientation of the magnetic field, velocity shear and perturbation wavevector play crucial role in assisting the instability. In the presence of only vertical field and vertical wavevector, ambipolar and Ohm diffusion can be combined together as Pedersen diffusion and causes only damping; in this case only Hall drift in tandem with shear flow drives the instability. However, for non-vertical field and oblique wavevector, both ambipolar diffusion and Hall drift assist the instability.

We investigate the stability of a magnetic element in the network and internetwork. The shear scale is not yet observationally determined and thus, assuming typical shear flow gradient $\sim 0.1 \text{ s}^{-1}$ we show that the magnetic diffusion shear instability grows over a minute. Thus, it is plausible that network–internetwork magnetic elements are subject to this fast growing, diffusive shear instability. This fast-growing instability could play important role in driving low frequency turbulence in the photosphere–chromosphere plasma.

Key words: Sun: Photosphere, MHD, waves.

1 INTRODUCTION

The solar atmosphere is host to a number of highly energetic events such as coronal mass ejections (CMEs), flares, prominences, coronal heating. The huge reservoir of energy in the solar atmosphere is related to the magnetic field originating in the convection zone where shearing motion of field line footpoints can stretch and twist the anchored field (Parker 1979). A variety of magnetohydrodynamic (MHD) waves are generated in the corona due to convective motion in the photosphere. The convective shearing motion not only produces Alfvén, fast or, slow magnetoacoustic waves, but, also, brings topologically disparate parts of magnetic configuration closer together resulting in the formation of current sheets. All in all, a tiny fraction of convective energy carried by the waves to higher altitude may suffice to

heat the coronal plasma to high temperatures. This simple physical picture of wave excitation, propagation and ensuing coronal heating is quite attractive since it ties the heat transport in the solar corona and heliosphere to the ultimate source of energy – the shearing photospheric convective motions. Therefore the investigation of wave propagation and concomitant heating of coronal plasma in the framework of MHD has been very popular topic in solar physics (Priest 1987; Parhi et al. 1997a,b, 1998; Hasan & Kalkofen 1999; Goedbloed & Poedts 2004; Aschwanden 2009).

Most solar atmospheric heating, with possible exception of flares, takes place in the chromosphere. The chromosphere is highly stratified and extends up to about nine pressure scale heights, i.e. about 2 Mm above the photospheric surface. The lower chromosphere is threaded by strong (\sim kiloGauss) vertical flux tubes located in the network regions

where they are observed as bright points. These tubes, which have a low filling factor ($< 1\%$) near the footpoint in the photosphere, expand to fill about 15% of the lower chromosphere ($\sim 1\text{Mm}$, where CaII emission features are observed in H and K lines) before filling the entire atmosphere forming a canopy in the chromosphere. The quiet solar internetwork region is also magnetised, with patches of kG field concentration (de Wijn et al. 2009; Almeida et al. 2010) and an order of magnitude smaller field everywhere else. Observation suggests that localised active regions that emit $\sim 80\%$ of the coronal radiative loss near solar maximum contain plasma of chromospheric origin (Aschwanden 2001). This fact raises the possibility that the same mechanism that transports mechanical energy from the convection zone to the chromosphere to sustain its heating rate also supplies the energy needed to heat the corona and accelerate the solar wind.

The absence of a unified theoretical framework to address the heating problem of the chromosphere–corona is partially related to the overuse of ideal MHD, from the deep interior of the sun to the corona. This approach is valid only for the fully ionised plasma in which field and fluid are *well* coupled to each other, a far cry from the low temperature photosphere–chromosphere where non-ideal MHD effects such as Hall, ambipolar and Ohm diffusion dominate (Pandey & Wardle 2006, 2008; Pandey et al. 2008; Khomenko & Collados 2012; Sykora et al. 2012; Pandey & Wardle 2012a). It is well known [Vernazza et al. (1981); hereafter VAL81] that the number of plasma particles in the partially ionised solar atmosphere, particularly below 2.5 Mm is small compared to the neutrals and thus, the plasma fluid is not frozen in the magnetic field but can slip through it due to frequent collisions with the neutrals (Mestel & Spitzer 1956).

The inclusion of neutral dynamics not only destroys the economy and simplicity of single fluid MHD description of fully ionised plasma but very concept of well defined flux tube may be difficult to define in the multi-fluid framework. Furthermore, high frequency Alfvén wave may not survive the collision dominated photosphere and chromosphere (Goodman 2004; Leake et al. 2005; Vranjes et al. 2007; Arber et al. 2007; Vranjes et al. 2008; Goodman 2011). This could have been anticipated on the ground that in the photosphere ($\lesssim 500\text{ km}$) and chromosphere ($\lesssim 2500\text{ km}$) the plasma number density is much smaller than the neutral number density and thus, high frequency (with respect to the ion-neutral collision frequency) MHD waves are severely damped by collisional dissipation of the wave energy. A way out of this difficulty is to retain the MHD momentum equation and include collisional effects by modifying the induction and energy equations via conductivity tensor (Erdelyi & James 2004; Leake & Arber 2006), an approach often employed to study the lower ionosphere of the Earth. However, derivation of the *time-independent* conductivity tensor requires the neglect of time derivatives in the electron and ion momentum equations, i.e. $d_{e,i}/dt \sim \omega_{e,i} \ll \omega_{ce,ci}$, implying plasma dynamical response frequency, $\omega_{e,i}$ is much smaller than their respective gyro-frequencies, $\omega_{ce,ci}$. Therefore, neglecting plasma inertia, a linear relationship between the electric field \mathbf{E} and plasma current \mathbf{J} can be easily derived $\mathbf{E} = \boldsymbol{\sigma} \cdot \mathbf{J}$ where $\boldsymbol{\sigma}$ is the *time-independent* conductivity tensor. However, equation of motion in the MHD frame-

work assumes $\omega_i \sim \omega_{ci}$. In fact ion carries the inertia of the fluid. Therefore, on the one hand, the *time-independent* conductivity tensor implies $\omega_{e,i} \ll \omega_{ce,ci}$, on the other hand, MHD momentum equation requires $\omega_i \sim \omega_{ci}$. Clearly, investigation of the collisional effects by merely modifying the induction and energy equation in the MHD framework is highly unsatisfactory.

Any realistic model of the solar atmosphere must reflect two basic observational facts: (a) the magnetic field distribution on the solar surface is not continuous but is organised in the network and internetwork elements. Whereas network field ($\gtrsim \text{kG}$) is predominantly vertical organised in the flux tubes (diameter $\lesssim 100\text{ km}$) located in the intergranular lanes, the internetwork field [\in (few G – kG)] in the interior of supergranule cells is mostly horizontal (Hasan 2009; Lites et al. 2008)¹; (b) plasma in the photosphere–chromosphere is weakly ionised [with fractional ionisation, which is a ratio of the electron and neutral number densities $X_e = n_e/n_n \sim 10^{-4}$, VAL81].

Both active and quiet phases of solar atmosphere are highly dynamic and consist of convectively driven vortices and flows of various spatial and temporal scales (Bonet et al. 2008; Wedemeyer-Böhm & Voort 2009; Balmaceda et al. 2010; Bonet et al. 2010). Most vortices are small ($\lesssim 0.5\text{ Mm}$) with average size $\sim 241 \pm 25\text{ km}$ and typical lifetime $\sim 3 - 5\text{ min.}$ though large vortices $\sim 20\text{ Mm}$ with lifetime $\gtrsim 20\text{ min.}$ have also been observed (Attie et al. 2009). The bright points associated with the vortex motion in the intergranular lane moves with typical speed $\lesssim 2\text{ km/s}$ (Wedemeyer-Böhm & Voort 2009). The magnetic fields appear to play crucial role in mediating vortex motion in the photosphere and chromosphere (Steiner & Rezaei 2012).

Rotation has been invoked in the past to explain the stability of flux tubes (Schüssler 1984). Models of spicules also use concept of rotating flux tubes (Kudoh & Shibata 1997). The numerical simulation of solar convection displays turbulent vortex flows at intergranular lanes (Zirker 1993; Stein & Nordlund 1998). The vorticity generation near boundaries of granules have also been seen in the numerical simulation of photosphere (Nordlund et al. 2009; Muthsam et al. 2010). The formation of small-scale, intergranular vortices suggests that vorticity is formed due to interaction of the photospheric plasma with ambient magnetic field in the intergranular lanes (Moll et al. 2011; Shelyag et al. 2011). The high resolution simulations of non-ideal MHD effects shows that Hall effect generates out-of-plane velocity fields with maximum speed $\sim 0.1\text{ km/s}$ at interface layers between weakly magnetized light bridges and neighbouring strong field umbral regions (Cheung & Cameron 2012). To summarise, both observation and numerical simulation points to the presence of shear flow at various spatial scales in the solar photosphere.

The large scale shear flow acts as a source of free energy in the solar plasma that can easily destabilise waves. For example, shear driven Kelvin-Helmholtz instability (KHI), which converts shear flow energy into vortex kinetic energy, is invoked to explain the instability of the flux tubes (Kolesnikov et al. 2004; Soler et al. 2010). Although solar

¹ Internetwork field could be as well isotropic (Almeida and González 2011), but see also Steiner & Rezaei (2012).

atmosphere may be susceptible to KHI (Karpen et al. 1993; Kolesnikov et al. 2004; Soler et al. 2010; Zaqarashvili et al. 2010; Ofman & Thompson 2011; Foullon et al. 2011), the presence of magnetic field is not conducive to this instability. For example, magnetic field along the flow suppresses KHI whereas transverse (to the flow) field has no effect on the instability (Chandrasekhar 1961). However, magnetic field not only quenches shear instabilities but can also facilitate it. For example, the most important instability in accretion discs, the magnetorotational instability is caused by an interplay between the Keplerian shear flow and magnetic field (Balbus & Hawley 1998). Thus, depending on the presence of flow gradient, magnetic field, when well coupled to the plasma can suppress as well as drive shear instabilities. Therefore, before dwelling upon the role of magnetic field on the shear driven instabilities, it is pertinent to know how well is magnetic field coupled to the surrounding matter.

The field drift through weakly ionised matter in the presence of shear flow can assist waves to grow. For example, in protoplanetary discs, both Hall and ambipolar diffusion assists magnetorotational instability (Wardle 1999; Balbus & Terquem 2001; Kunz & Balbus 2004; Desch 2004; Wardle & Salmeron 2011; Pandey & Wardle 2012b). Clearly, drift of the magnetic field in a weakly ionised diffusive medium provides new pathways through which shear energy can be channelled to the waves. However, the role of diffusion in destabilising partially ionised medium in the presence of shear flow is not unique to weakly ionised discs but is quite generic (Kunz 2008; Pandey & Wardle 2012a). The crucial ingredients required to excite this diffusion–shear instability is: (a) the presence of a shear flow, and, (b) *favourable* magnetic field topology. The ensuing instability is overtly similar to KHI, and not surprisingly, the growth rate is proportional to the shear gradient. However, unlike KHI which is hydrodynamic in nature, this is magnetohydrodynamic instability.

A detailed investigation of diffusive shear instability in the context of solar atmosphere is carried out in the present work which although similar to our previous work [Pandey & Wardle (2012a), hereafter PW12a] has following notable differences. (i) Unlike PW12a, where only vertical field and transverse fluctuation (vertical wavevector) is assumed, in the present case field topology is more general and wavevector is oblique; (ii) In PW12a back reaction of the fluid on the magnetic field was completely ignored. By retaining the back reaction of the fluid on the field we show that shear driven diffusive instability do not have any cut-off wavelength; (iii) For vertical field and transverse fluctuations we showed in PW12a that only Hall diffusion assists the instability and ambipolar and Ohm, which combines as Pedersen diffusion only causes damping of waves. In the present work for general field topology and oblique wavevector, we shall see that both ambipolar and Hall diffusion can assist the instability; (iv) The general stability criterion for magnetic diffusion dominated plasma in the presence of shear flows is presented in this work. Therefore, this paper is more general in scope and application than PW12a.

The paper is organised in the following fashion. The basic set of equations and dispersion relation is given in Sec. 2. In subsection 2.1 we give linearised equations in terms of diffusion tensor before describing general dispersion relation. In Sec. 3 the general stability criterion is described and maxi-

mum growth rate of the instability is derived. The expression for maximum growth rate and critical wavelength is given in various limiting cases. In Sec. 4, various limiting cases of the dispersion relation is discussed. In Sec. 5 application of the result is discussed. Finally, in Sec. 6 brief summary of the result is given.

2 BASIC MODEL

The photosphere–chromosphere plasma consists of electrons, protons, singly ionized metallic ions, H, He I, He II, and He III. We shall ignore the distinction between hydrogen and metallic ions and assume that photosphere–chromosphere is made up of electrons, singly charged ions and neutral Hydrogen. Although basic set of equations for partially ionised plasma was formulated more than 50 years ago (Cowling 1957; Braginskii 1965), we shall use the single fluid formulation given by Pandey & Wardle (2008) for which the spatial and temporal scales of partially ionised plasma has been clearly elucidated.

In the low frequency limit, the collisional dynamics and fractional ionisation can be incorporated in the basic set of equations without having to deal with the complexity of three–fluid equations. Thus the continuity equation of the bulk plasma fluid is

$$\frac{\partial \rho}{\partial t} + \nabla \cdot (\rho \mathbf{v}) = 0. \quad (1)$$

Here $\rho = \rho_i + \rho_n$ is the bulk mass density and $\rho_{i,n} = m_{i,n} n_{i,n}$ is the ion and neutral mass densities with $m_{i,n}, n_{i,n}$ as the ion and neutral mass and number densities respectively; $\mathbf{v} = (\rho_i \mathbf{v}_i + \rho_n \mathbf{v}_n)/\rho$ is the bulk velocity, and, \mathbf{v}_i and \mathbf{v}_n are bulk velocities of the ion and neutral fluids respectively. The momentum equation is

$$\rho \frac{d\mathbf{v}}{dt} = -\nabla P + \frac{\mathbf{J} \times \mathbf{B}}{c}, \quad (2)$$

where $\mathbf{J} = e n_e (\mathbf{v}_i - \mathbf{v}_e)$ is the current density, \mathbf{B} is the magnetic field and $P = P_e + P_i + P_n$ is the total pressure. The induction equation is

$$\frac{\partial \mathbf{B}}{\partial t} = \nabla \times \left[(\mathbf{v} \times \mathbf{B}) - \frac{4\pi\eta_O}{c} \mathbf{J} - \frac{4\pi\eta_H}{c} \mathbf{J} \times \mathbf{b} + \frac{4\pi\eta_A}{c} (\mathbf{J} \times \mathbf{b}) \times \mathbf{b} \right], \quad (3)$$

where $\mathbf{b} = \mathbf{B}/B$ is the unit vector along the magnetic field, and Ohm (η_O), ambipolar (η_A) and Hall (η_H) diffusivities are

$$\eta_O = \frac{c^2}{4\pi\sigma}, \eta_A = \frac{D^2 B^2}{4\pi\rho_i \nu_{in}}, \eta_H = \frac{cB}{4\pi e n_e}. \quad (4)$$

Here

$$\sigma = \frac{c e n_e}{B} \left[\frac{\omega_{ce}}{\nu_e} + \frac{\omega_{ci}}{\nu_i} \right] \quad (5)$$

is the parallel conductivity, $\omega_{cj} = eB/m_j c$ is the particle's cyclotron frequency where e, B, m_j, c denotes the charge, magnetic field, mass and speed of light respectively and $D = \rho_n/\rho$ is the ratio of neutral and bulk densities. For electrons $\nu_e = \nu_{en}$ and for ions $\nu_i \equiv \nu_{in}$. Although $\nu_{ee}, \nu_{ei}, \nu_{ii}$ and ν_{ie} can become comparable to ν_{en} (see Table. 1), it is the neutral-plasma collision that gives rise to ambipolar and

Hall diffusion in the medium.² The electron-ion collision contributes to Ohm diffusion.

Defining the plasma Hall parameter β_j as

$$\beta_j = \frac{\omega_{cj}}{\nu_{in}}, \quad (6)$$

and the Hall frequency

$$\omega_H = \frac{\rho_i}{\rho} \omega_{ci}, \quad (7)$$

the diffusivities in Eq. (4) can be written in the compact form (Pandey & Wardle 2008)

$$\eta_H = \left(\frac{v_A^2}{\omega_H} \right), \eta_A = D \left(\frac{v_A^2}{\nu_{ni}} \right), \text{ and } \eta_O = \beta_e^{-1} \eta_H, \quad (8)$$

where $\nu_{ni} = \rho_i \nu_{in} / \rho_n$ and $v_A = B / \sqrt{4\pi\rho}$.

The induction Eq. (3) can be explicitly written in terms of fluid and field velocities as (Wardle & Salmeron 2011)

$$\frac{\partial \mathbf{B}}{\partial t} = \nabla \times \left[(\mathbf{v} + \mathbf{v}_B) \times \mathbf{B} - \frac{4\pi\eta_O}{c} \mathbf{J}_{\parallel} \right]. \quad (9)$$

where the field drift velocity \mathbf{v}_B is

$$\mathbf{v}_B = \eta_P \frac{(\nabla \times \mathbf{B})_{\perp} \times \mathbf{b}}{B} - \eta_H \frac{(\nabla \times \mathbf{B})_{\perp}}{B}, \quad (10)$$

and

$$\eta_P = \eta_O + \eta_A, \quad (11)$$

is the Pedersen diffusivity. The parallel and perpendicular components of current in the preceding equation refer to the orientation with respect to the background magnetic field. In the fluid frame, the magnetic drift velocity \mathbf{v}_B contains effect of field diffusion. As we shall see, the induction Eq. (9) in terms of magnetic drift velocity is particularly convenient for linearization which we will do shortly.

We note from Eq. (4) that Ohm diffusion is independent of the magnetic field. Whereas Hall has linear dependence on the field, i.e. $\eta_H \propto B$, the dependence of ambipolar diffusion on the magnetic field is quadratic, i.e. $\eta_A \propto B^2$. Thus, as the magnetic field strength in a flux tube decreases with increasing altitude, the drop in the Hall diffusivity will not be as severe as in ambipolar diffusion. The altitude dependence of diffusivities can be easily quantified if variation of the magnetic field with altitude is known. Thus, in order to compute diffusivities at various altitude, we shall choose power law variation of the magnetic field with neutral number density n_n

$$B = B_0 \left(\frac{n_n}{n_0} \right)^{0.3}, \quad (12)$$

where n_0 is the number density of neutrals at the surface ($h = 0$) and $B_0 = 1.2$ kG is the typical value of the field at intergranular boundaries. Such a field profile captures essential height dependence of observed field in flux tubes (Martinez et al. 1997). We note that above scaling of the magnetic field differs somewhat from the mass density scaling (Leake et al. 2005) although we have retained the same power law index 0.3.

The value of neutral number density and fractional ionisation (Model C, VAL81), the ratio of neutral and bulk

² To leading order collisions between like plasma particles ν_{ee} , ν_{ii} do not cause diffusion (Longmire & Rosenbluth 1956).

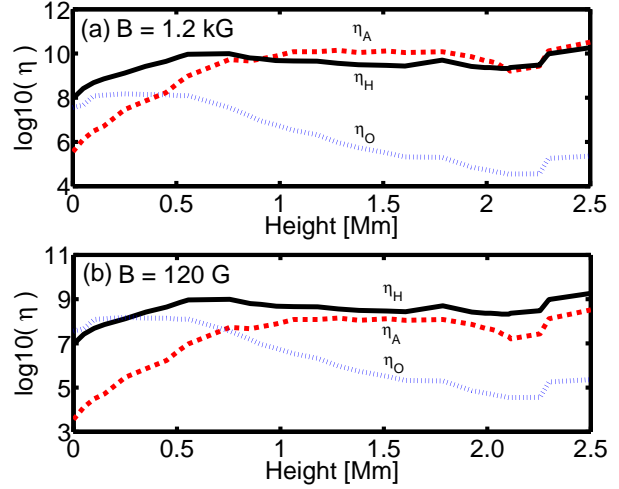


Figure 1. The Ohm (η_O), Hall (η_H) and ambipolar (η_A) diffusion profiles in the photosphere-chromosphere are shown for (a) $B = 1.2$ kG and (b) $B = 120$ G.

densities D , and, various collision frequencies are given in Table 1. The collision cross-section is not known for the metallic ions-neutral collision, so we have employed the Messy-Mohr analytic formula for the cross-section (see appendix). The resulting plasma-neutral collision frequency in the present work is an order of magnitude smaller than previously used values by Pandey et al. (2008) where a larger plasma-neutral collision cross-section was assumed for ion – H_2 collision.

We shall utilise the above magnetic field profile, along with the collision frequencies given in Table 1 to compute diffusivities which are given in Table 2. In Fig 1 diffusivities are plotted against height which shows that Hall diffusion dominates Ohm and ambipolar diffusion in the photosphere and lower chromosphere in the intense field regions [Fig 1(a)]. However in the weak field (~ 100 G at $h = 0$) regions Ohm and Hall are comparable below 0.3 Mm before Hall becomes dominant diffusion in the entire photosphere-chromosphere [Fig 1(b)].

It has been suggested in the past that Pedersen diffusion (which is the sum of Ohmic and ambipolar diffusions) could play an important role in the chromospheric heating (Goodman 2004). We find that in the sunspots, active regions, pores and intergranular regions where field is intense, Hall and ambipolar will dominate Ohm diffusion. Clearly realistic modelling of various energetic processes such as chromospheric heating, CMEs etc. must include these diffusive processes. It would appear that since Hall diffusion is non-dissipative in nature, it may not have any role in the energy extraction from the convective motion of the largely neutral medium. However, as we have shown recently (Pandey & Wardle 2012a), Hall diffusion in the presence of shear flow destabilises low frequency fluctuations which in turn may lead to the turbulent cascade of convective energy to smaller scales where dissipation can convert it to heat. Therefore, it is quite plausible that the Hall effect may play an important role in heating the chromospheric plasma.

How much diffusion is too much in the solar atmosphere? For example, if magnetic diffusion dominates fluid

Table 1. The neutral number density n_n , the fractional ionisation $X_e \equiv n_e/n_n$ [Model C, VAL81], the ratio of neutral to bulk mass densities $D = \rho_n/\rho$, the ion-neutral, electron-neutral, and electron-ion collision frequencies are given in the table. We have assumed $B = B_0 (n_n/n_0)^{0.3}$ with $B_0 = 1.2$ kG and $m_i = 30 m_p$ and $m_n = 2.3 m_p$ where $m_p = 1.67 \times 10^{-24}$ g is the proton mass.

h (km)	$n_n(\text{cm}^{-3})$	X_e	D	ν_{in} (Hz)	ν_{en} (Hz)	ν_{ei} (Hz)
0	$1.2 \cdot 10^{17}$	$5.5 \cdot 10^{-3}$	1	10^8	$7.4 \cdot 10^9$	$1.3 \cdot 10^9$
250	$2.3 \cdot 10^{16}$	10^{-4}	1	10^7	$1.3 \cdot 10^9$	$1.2 \cdot 10^8$
515	$2.1 \cdot 10^{15}$	$1.2 \cdot 10^{-4}$	1	10^6	10^9	$1.3 \cdot 10^7$
1065	$1.7 \cdot 10^{13}$	10^{-2}	0.91	10^4	10^6	$3.1 \cdot 10^6$
1515	10^{12}	$6 \cdot 10^{-2}$	0.53	$8 \cdot 10^2$	$6.6 \cdot 10^4$	$2.0 \cdot 10^6$
2050	$7.7 \cdot 10^{10}$	$5 \cdot 10^{-1}$	0.12	60	$5.3 \cdot 10^3$	$9.6 \cdot 10^5$
2298	$3.2 \cdot 10^9$	$1 \cdot 10^0$	0.07	6.3	10^3	10^5
2543	10^9	$1.2 \cdot 10^0$	0.05	6.3	$5.3 \cdot 10^2$	$3.2 \cdot 10^2$

Table 2. The values of Ohm, η_O , ambipolar, η_A and Hall, η_H diffusivities at different altitude are given in the table. The value of various collision frequencies have been taken from Table 1.

h (km)	$\eta_O(\text{cm}^2/\text{s})$	$\eta_A(\text{cm}^2/\text{s})$	$\eta_H(\text{cm}^2/\text{s})$	h (km)	$\eta_O(\text{cm}^2/\text{s})$	$\eta_A(\text{cm}^2/\text{s})$	$\eta_H(\text{cm}^2/\text{s})$
0	$3.6 \cdot 10^7$	$3.6 \cdot 10^5$	$9.3 \cdot 10^7$	1180	$2.1 \cdot 10^6$	$1.2 \cdot 10^{10}$	$4.5 \cdot 10^9$
100	$1.2 \cdot 10^8$	$3.1 \cdot 10^6$	$4.8 \cdot 10^8$	1380	$5.5 \cdot 10^5$	$1.1 \cdot 10^{10}$	$3.1 \cdot 10^9$
250	$1.5 \cdot 10^8$	$2.9 \cdot 10^7$	$1.3 \cdot 10^9$	1605	$2.1 \cdot 10^5$	$1.1 \cdot 10^{10}$	$2.7 \cdot 10^9$
515	$1.2 \cdot 10^8$	$5.2 \cdot 10^8$	$7.1 \cdot 10^9$	1925	$7.3 \cdot 10^4$	$7.2 \cdot 10^9$	$2.6 \cdot 10^9$
555	$1.2 \cdot 10^8$	$9.4 \cdot 10^8$	$9.2 \cdot 10^9$	2016	$5.1 \cdot 10^4$	$4.4 \cdot 10^9$	$2.3 \cdot 10^9$
755	$3.6 \cdot 10^7$	$5.3 \cdot 10^9$	$9.8 \cdot 10^9$	2104	$3.5 \cdot 10^4$	$2 \cdot 10^9$	$2.1 \cdot 10^9$
855	$1.5 \cdot 10^7$	$4.6 \cdot 10^9$	$6.3 \cdot 10^9$	2255	$3.6 \cdot 10^4$	$2.7 \cdot 10^9$	$3 \cdot 10^9$
980	$5.9 \cdot 10^6$	$7.6 \cdot 10^9$	$4.8 \cdot 10^9$	2543	$2.4 \cdot 10^5$	$4 \cdot 10^{10}$	$2.1 \cdot 10^{10}$

convection in the induction Eq. (3), field will be poorly coupled to the plasma (Wardle 2007). Thus, we shall compare advection term $\nabla \times (\mathbf{v} \times \mathbf{B}) \sim vB/L$ with various diffusion term in the induction Eq. (3) by defining magnetic Reynolds numbers R_m , A_m and H_m as

$$R_m = \frac{vL}{\eta_O}, A_m = \frac{vL}{\eta_A} \text{ \& } H_m = \frac{vL}{\eta_H}. \quad (13)$$

Note that both A_m and H_m depends on how well the plasma is coupled to the magnetic field since both ambipolar and Hall diffusion depends on the magnetic field. Further $\eta_A = \beta_i \eta_H$ and $\eta_H = \beta_e \eta_O$. Thus

$$A_m = R_m/(\beta_i \beta_e), \quad H_m = R_m/\beta_e. \quad (14)$$

The dependence of A_m and H_m on the plasma Hall parameter β_j is not surprising since the origin of both ambipolar and Hall diffusion is inherently linked to the magnetisation of the medium. This also explains inherently different nature of the Ohm and ambipolar diffusion: whereas Ohm diffusion acts isotropically, ambipolar diffusion owing to its dependence on the magnetic field is anisotropic. As we shall see, in the presence of shear flow, the anisotropic nature of ambipolar diffusion is at the centre of wave destabilization.

The height dependence of R_m , H_m and A_m for both kG and 0.1 kG fields were discussed in PW12a. It was shown that when $v \sim v_A$ (where v_A is the Alfvén speed), $R_m \gg 1$ suggesting that the Ohm diffusion is unimportant in comparison with the advection term. However, H_m and A_m are three to four orders of magnitude smaller than R_m . The recent 2D numerical simulation of partially ionized solar atmosphere also suggests that in the weak field ($\lesssim 100$ G) regions in the chromosphere, the Hall diffusion is two orders of magnitude larger than the Ohm diffusion whereas ambipolar diffusion is four to six order of magnitude larger

than the Ohm diffusion (Sykora et al. 2012). Clearly, both ambipolar and Hall diffusion terms are important in the induction equation.

2.1 Dispersion relation

The magnetic element in the photosphere-chromosphere which can be modelled as cylindrical tubes or planer sheets are highly dynamic accompanied by numerous flows with different spatial/ temporal scales. Recent numerical simulations of the umbral magneto convection suggests that the dynamical scale over which Hall diffusion can generate magnetic and velocity fields is much faster [~ 10 – 20 km spatial scale and ~ 300 s temporal scale (Cheung & Cameron 2012)] than the spatial and temporal scale of a typical flux tube (\gtrsim few hundred km and \sim few days). The simulation results are easily scalable to 2 km with temporal scale ~ 2 s. We note that at present the best achievable resolution is 90 km (Bonet et al. 2008).

Since the spatial scale over which the flow and field generation occurs, is much smaller than the typical tube diameter, we shall approximate the cylindrical tube by a planer sheet and work in the Cartesian coordinate system where x, y, z represents radial, azimuthal and vertical directions locally. We shall assume an initial homogeneous state with azimuthal shear flow $\mathbf{v} = v_0' x \mathbf{y}$. The magnetic field in the intergranular lanes at the network boundaries is clumped into elements or flux tubes that are generally vertical (Martinez et al. 1997; Hasan 2009) but highly inclined fields have also been reported in the literature (Stenflo et al. 1987; Solanki et al. 1987). The internetwork magnetic elements have predominantly horizontal field (Hasan 2009; Steiner & Rezaei 2012). Therefore, we shall assume uniform

background field that have both azimuthal as well as vertical component, i.e. $\mathbf{B} = (0, B_y, B_z)$.

The focus of the present investigation is low frequency behaviour of the medium, and thus, we shall work in the Boussinesq approximation limit which is valid if the motion in the medium is very slow (Spiegel & Veronis 1960). Thus linearising Eqs. (1) and (2) and assuming an axisymmetric perturbations of the form $\exp(i\mathbf{k} \cdot \mathbf{x} + \sigma t)$, with $\mathbf{k} = (k_x, 0, k_z)$, in Boussinesq approximation, we get

$$\mathbf{k} \cdot \delta \mathbf{v} = 0. \quad (15)$$

$$\begin{aligned} \sigma \delta v_x &= -i k_x \frac{\delta p}{\rho} + \frac{i}{4\pi\rho} [(\mathbf{k} \cdot \mathbf{B}) \delta B_x - (\mathbf{B} \cdot \delta \mathbf{B}) k_x], \\ \sigma \delta v_y + v'_0 \delta v_x &= \frac{i}{4\pi\rho} (\mathbf{k} \cdot \mathbf{B}) \delta B_y, \\ \sigma \delta v_z &= -i k_z \frac{\delta p}{\rho} + \frac{i}{4\pi\rho} [(\mathbf{k} \cdot \mathbf{B}) \delta B_z - (\mathbf{B} \cdot \delta \mathbf{B}) k_z]. \end{aligned} \quad (16)$$

Eliminating the pressure perturbation in favour of velocity and making use of Eq. (15), from preceding equation we get for the (x, y) components

$$\delta \hat{\mathbf{v}} = \frac{i k v_A \mu}{\sigma^2} \begin{pmatrix} \sigma & 0 \\ -v'_0 & \sigma \end{pmatrix} \delta \hat{\mathbf{B}}. \quad (17)$$

Here $\delta \hat{\mathbf{v}} = \delta \mathbf{v}/v_A$ and $\delta \hat{\mathbf{B}} = \delta \mathbf{B}/B$, $v'_0 = dv(x)/dx$, $\mu = (\hat{\mathbf{k}} \cdot \mathbf{b}) \equiv \hat{k}_z b_z$, $\tilde{k} = \mathbf{k}/k$ and $\hat{k}_z = k_z/k$. Since

$$\begin{aligned} \delta \mathbf{v}_B &= i k \left[\eta_H \left\{ \mu \delta \hat{\mathbf{B}} \times \mathbf{b} - (\mathbf{b} \cdot \delta \hat{\mathbf{B}}) \tilde{k} \times \mathbf{b} \right\} \right. \\ &\quad \left. + \eta_P \left\{ \mu \delta \mathbf{B} - (\mathbf{b} \cdot \delta \hat{\mathbf{B}}) \tilde{k} \right\} \right], \end{aligned} \quad (18)$$

the linearised induction equation (x, y components) can be written as

$$\begin{aligned} \left[\begin{pmatrix} \sigma & 0 \\ -v'_0 & \sigma \end{pmatrix} + \frac{k^2 v_A^2 \mu^2}{\sigma^2} \begin{pmatrix} \sigma & 0 \\ -v'_0 & \sigma \end{pmatrix} \right. \\ \left. + k^2 \begin{pmatrix} \eta_{xx} & \eta_{xy} \\ \eta_{yx} & \eta_{yy} \end{pmatrix} \right] \delta \hat{\mathbf{B}} = 0, \end{aligned} \quad (19)$$

where $\boldsymbol{\eta}$ is the diffusivity tensor with following components

$$\begin{aligned} \eta_{xx} &= \eta_O + b_z^2 \eta_A, \quad \eta_{xy} = s \eta_H + g \eta_A, \\ \eta_{yx} &= (g \eta_A - s \eta_H) / \hat{k}_z^2, \quad \eta_{yy} = \eta_O + \left(1 - \hat{k}_x^2 b_z^2\right) \eta_A, \end{aligned} \quad (20)$$

Here

$$g = -\hat{k}_x \hat{k}_z b_y b_z, \quad (21)$$

and helicity $s = \mu \hat{k}_z \equiv b_z \hat{k}_z^2$. We note that for purely vertical field the sign of helicity s is determined by the projection of the vertical magnetic field on the vorticity, $\nabla \times \mathbf{v}_0$.

Following dispersion relation can be derived from (19)

$$\tilde{\sigma}^4 + \tilde{k}^2 (\tilde{\eta}_P + \tilde{\eta}_T) \tilde{\sigma}^3 + C_2 \tilde{\sigma}^2 + C_1 \tilde{\sigma} + C_0 = 0, \quad (22)$$

where

$$\begin{aligned} C_2 &= \tilde{k}^4 (\tilde{\eta}_P \tilde{\eta}_T + \mu^2 \tilde{\eta}_H^2) + \tilde{k}^2 [2\mu^2 - \alpha (g \tilde{\eta}_A + s \tilde{\eta}_H)], \\ C_1 &= \tilde{k}^4 \mu^2 (\tilde{\eta}_P + \tilde{\eta}_T), \\ C_0 &= \tilde{k}^4 \mu^2 [\mu^2 - \alpha (g \tilde{\eta}_A + s \tilde{\eta}_H)], \end{aligned} \quad (23)$$

$$\alpha = -v'_0 / |v'_0| \equiv \pm 1 \text{ and}$$

$$\eta_T = \eta_O + \mu^2 \eta_A. \quad (24)$$

We have used following normalisation in the above equations

$$\tilde{\sigma} = \frac{\sigma}{|v'_0|}, \quad \tilde{k} = \frac{k v_A}{|v'_0|}, \quad \tilde{\eta} = \frac{\eta |v'_0|}{v_A^2}. \quad (25)$$

Eq. (22) reduces to known dispersion relation (Kunz 2008) when $D = 1$ and $\eta_O = 0$. When $D = 0$, ambipolar diffusion expectedly, drops out of the dispersion relation.

3 NON-IDEAL MHD INSTABILITIES

A general stability criterion in the magnetic diffusion dominated plasma can be derived from the dispersion relation, Eq. (22) by recasting it in the following simple form

$$a \tilde{k}^4 + b \tilde{k}^2 + c = 0, \quad (26)$$

where the coefficients a , b and c are

$$a = \beta - \gamma \mu^2, \quad b = \delta - \gamma \tilde{\sigma}^2, \quad c = \tilde{\sigma}^4, \quad (27)$$

with

$$\begin{aligned} \beta &= (\mu^2 \tilde{\eta}_H^2 + \tilde{\eta}_P \tilde{\eta}_T) \tilde{\sigma}^2 + (\tilde{\eta}_P + \tilde{\eta}_T) \mu^2 \tilde{\sigma} + \mu^4, \\ \delta &= [(\tilde{\eta}_P + \tilde{\eta}_T) \tilde{\sigma} + 2\mu^2] \tilde{\sigma}^2, \\ \gamma &= \alpha (g \tilde{\eta}_A + s \tilde{\eta}_H). \end{aligned} \quad (28)$$

The dispersion relation, Eq. (26) can also be recast as

$$\beta \tilde{k}^4 + \delta \tilde{k}^2 + \tilde{\sigma}^4 = \gamma \tilde{k}^2 [\tilde{\sigma}^2 + \mu^2 \tilde{k}^2]. \quad (29)$$

Thus in the neighbourhood of $\tilde{\sigma} \sim \tilde{k} \ll 1$ where

$$\beta \sim \mu^4, \quad \delta \sim 2\mu^2 \tilde{\sigma}^2, \quad (30)$$

Eq. (29) becomes

$$\mu^2 \tilde{k}^2 + \tilde{\sigma}^2 = \gamma^2 \tilde{\sigma}^2, \quad (31)$$

which can be written as

$$\gamma - \mu^2 = \left(\frac{\tilde{\sigma}}{\tilde{k}} \right)^2. \quad (32)$$

From Eq. (32) we see that for positive σ right hand side is positive. This implies that $\gamma - \mu^2 > 0$. Therefore, we arrive at the general stability criterion which states that if

$$\alpha (g \tilde{\eta}_A + s \tilde{\eta}_H) > \mu^2, \quad (33)$$

the waves are unstable in the medium. The Ohm diffusion do not appear in the above expression which is not surprising considering that the above criterion pertains to the long wavelength fluctuations. For definiteness, in subsequent analysis, we shall assume $\alpha = 1$.

The diffusion-shear instability is caused by a competition between the fluid advection and field drift in the plasma. This can be seen from the y and x components of Eqs. (17) and (18) respectively, which suggest that when $\sigma = 0$, the advection of fluid in the x direction, $\delta \hat{v}_x$ is equal and opposite to the magnetic field drift velocity $\delta \hat{\mathbf{v}}_{Bx}$. By combining y component of Eqs. (17) and x component of Eq. (18)] we get

$$\delta \hat{v}_x + \delta \hat{\mathbf{v}}_{Bx} = i \tilde{k} \mu \left[\frac{-\gamma + \mu^2}{\alpha \mu^2} \delta \hat{\mathbf{B}}_y + \frac{1}{\tilde{k}_z^2} \tilde{\eta}_A \delta \hat{\mathbf{B}}_x \right]. \quad (34)$$

Here we have neglected Ohm diffusion. By setting $-\gamma + \mu^2 = 0$ near marginal state, in the vicinity of $\tilde{\eta}_A \ll 1$, we get

$\delta \hat{v}_x + \delta \hat{v}_{Bx} \approx 0$. This provides a simple physical explanation on how the magnetic diffusion helps the shear flow in destabilising the waves. The outward slippage of the field in the x -direction due to magnetic diffusion weakens the magnetic tension force. As a result magnetic restoring force in the wave is dominated by the inertia force, resulting in the increased inward drift of the fluid elements. This is how magnetic diffusion assist the waves to grow in the presence of shear flow.

The stability criterion, Eq. (33) in the dimensional form becomes

$$-v'_0 (g \eta_A + s \eta_H) > \mu^2 v_A^2, \quad (35)$$

which suggests that when $-v'_0 > 0$, the linear combination of ambipolar and Hall diffusivities multiplied by suitable topological factors g and s must exceed square of the oblique Alfvén speed. Above equation provides a simple stability criterion of diffusive medium. For example, low frequency fluctuations in the Hall–Ohm dominated photosphere-lower chromosphere ($\eta_A = 0$) are unstable if

$$-v'_0 \eta_H > b_z v_A^2, \quad (36)$$

or, in terms of Hall frequencies

$$-v'_0 > b_z \omega_H \equiv \omega_{HZ}. \quad (37)$$

Here we have used $\eta_H = v_A^2/\omega_H$ (PW12a) and $b_z \omega_H = \omega_{HZ}$ is the Hall frequency defined in term of vertical field. Clearly if the Hall frequency is less than the shear frequency $-v'_0$, Hall diffusion can drive shear flow instability.

When $v'_0 \eta_H/v_A^2 = -b_z$, since $\eta_A > 0$, ambipolar diffusion can drive shear flow instability provided $g > 0$. For purely vertical field or, transverse fluctuations (vertical wavevector) when $g = 0$, ambipolar diffusion can only cause the damping of waves. Therefore, the question of ambipolar diffusion assisting the shear flow instability is inherently linked to the ambient field geometry and wave obliqueness which together is encapsulated in the topological factor g . The important role of g in the ambipolar diffusion driven shear flow instability was discovered by Desch (2004).

How does ambipolar diffusion help drive shear flow instability? In order to see this, we first note that when the wavevector is perfectly aligned to the ambient magnetic field, i.e. $\mu \equiv \hat{k}_z b_z = 1$, $\eta_T \equiv \eta_P$ in Eqs. (22)–(24), Ohm and ambipolar diffusion combines together as Pedersen diffusion and their effect on the wave propagation is identical—they both cause wave damping. Only when $\mu \neq 1$, this diffusive degeneracy is lifted and Ohm and ambipolar diffusion can no longer be combined together as single diffusion. After removal of degeneracy whereas Ohm diffusion still causes isotropic damping of the waves, damping by the ambipolar diffusion becomes anisotropic. Therefore, the non-vertical magnetic field and oblique wavevector (which is crucial in removing this degeneracy) plays important role in the ambipolar diffusion driven shear instability. This can also be seen from the generalised induction Eq. (3) if we rewrite the electric field as

$$\mathbf{E}' = \frac{4\pi}{c^2} \{ \eta_O + [1 - (\mathbf{j} \cdot \mathbf{b})^2] \eta_A \} \mathbf{J} + \frac{4\pi}{c^2} \eta_H \mathbf{J} \times \mathbf{b} + \frac{4\pi}{c^2} \eta_A (\mathbf{j} \cdot \mathbf{b}) [\mathbf{J} \times (\mathbf{J} \times \mathbf{b})], \quad (38)$$

where the electric field is written in the neutral frame, $\mathbf{j} = \mathbf{J}/|\mathbf{J}|$. It is clear from the preceding equation that when

medium is threaded only by the vertical field and wave is propagating along the field, i.e. $\mathbf{k} = (0, 0, k_z)$, $\mathbf{j} = (j_x, j_y, 0)$, both Ohm and ambipolar diffusion cause damping of the waves since $(\mathbf{j} \cdot \mathbf{b}) = 0$ and $\mathbf{E}' \cdot \mathbf{J} = \eta_P \mathbf{J}^2$. However, when $\mu \neq 1$, last term in Eq. (38) can help fluctuations grow since

$$\mathbf{E}' \cdot \mathbf{J} = \frac{4\pi}{c^2} \{ \eta_O + [1 - (\mathbf{j} \cdot \mathbf{b})^2] \eta_A \} \mathbf{J}^2 + \frac{4\pi}{c^2} \eta_A (\mathbf{j} \cdot \mathbf{b}) [\mathbf{J} \cdot (\mathbf{J} \times (\mathbf{J} \times \mathbf{b}))]. \quad (39)$$

Therefore, ambipolar diffusion plays dual role in a partially ionized medium: whereas, in one direction it can cause dissipation like Ohm, in the other direction the dissipation is considerably smaller. The directional dissipation is the hall mark of ambipolar diffusion which causes it to assist the instability (Desch 2004).

From stability criterion Eq. (35) it is clear that the Hall–Ohm stable medium ($-v'_0 \eta_H \leq b_z v_A^2$) may or may not be ambipolar unstable whereas Hall–Ohm unstable medium ($-v'_0 \eta_H > b_z v_A^2$) can always become ambipolar unstable for non-vertical field and oblique wavevector since $g > 0$ can be easily satisfied. The ambipolar diffusion not only drives shear flow instability when $g > 0$, but also enlarges the parameter space over which Hall can destabilise the waves. Therefore Hall diffusion can drive shear flow instability when

$$\eta_H > \frac{b_z v_A^2}{-v'_0} - \frac{g}{s} \eta_A. \quad (40)$$

Since $b_z, b_y \in [0, 1]$ and maximum $g = 0.25$, above inequality implies that for non-zero η_A , Hall diffusion drives shear instability at much larger negative value than when the field has only vertical component.

The stability criterion can also be recast as

$$-\left(\frac{\hat{k}_x}{\hat{k}_z} \frac{b_y}{b_z} \right) > \frac{1}{\eta_A} \left(\frac{v_A^2}{-v'_0} - \frac{1}{b_z} \eta_H \right). \quad (41)$$

Assuming positive left hand side in the preceding equation we see that above criterion is easily satisfied for non-zero η_A when $\hat{k}_z \rightarrow 0$. Therefore, waves propagating almost along x direction i.e. when the fluctuations are almost magnetosonic are always unstable.

The maximum growth rate of the instability can be found by setting the discriminant $b^2 - 4ac = 0$ in Eq. (26). This yields

$$\tilde{\sigma}_0 = \frac{g \eta_A + s \eta_H}{[(\eta_P + \eta_T) + 2 \sqrt{\mu^2 \eta_H^2 + \eta_P \eta_T}]}. \quad (42)$$

We see that the maximum growth rate depends on both $g \eta_A$ and $s \eta_H$ and for comparable η_A and η_H [as is the case in large part of the solar atmosphere; see Fig. (1)], the bigger contribution to the growth rate comes from the Hall diffusion since the maximum value of parameter g is 0.25 whereas maximum value of the helicity s is one.

In the absence of Hall and Ohm, the maximum growth rate, Eq. (42) becomes

$$\sigma_0 = \frac{g |v'_0|}{(1 + \mu)^2}, \quad (43)$$

which suggests that when the field drift is solely due to the ambipolar diffusion the maximum growth rate is independent of the diffusivity as well as the strength of the background magnetic field. However, the signature of the mag-

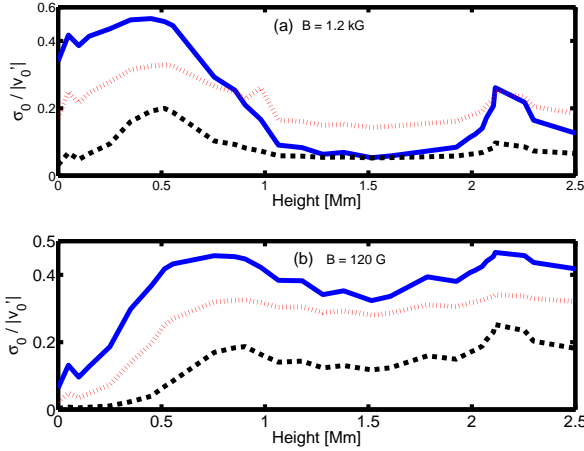


Figure 2. The maximum growth rate, Eq. (42) is shown for $\hat{k}_z = b_z = 1$ (bold line), $\hat{k}_z = \hat{k}_x = b_z = -b_y = 1/\sqrt{2}$ (dotted line) and $\hat{k}_z = 1/\sqrt{2}$ and $b_z = 0.1$ (dashed line) for (a) $B = 1.2$ kG and (b) $B = 120$ G.

netic field in Eq. (43) appears through the topological factors g and μ .

When the field drift in the plasma is solely due to the Hall diffusion, the maximum growth rate Eq. (42) becomes

$$\sigma_0 = \frac{|v'_0|}{2} \hat{k}_z, \quad (44)$$

which implies that the waves with $\hat{k}_z = 1$ are most unstable. A comparison with Eq. (43) shows that in purely ambipolar or, purely Hall case, growth rate is independent of the ambient diffusivity.

We see from Fig. 2(a) that for purely vertical field and vertical wavevector ($\hat{k}_z = b_z = 1$, $g = 0$, bold lines) the instability grows at maximum rate $|v'_0|/2$ in the photosphere-lower chromosphere in the strong field region. Recall that in this interval Hall is the dominant diffusion mechanism in the network and internetwork regions (Fig. 1) and dissipation due to the Ohm and ambipolar diffusion (which can be combined together as Pedersen diffusion for this topology) is small.

When the field is weak [Fig. 2(a)] the instability grows at close to maximum rate in the entire photosphere-chromosphere except very close to the surface ($\lesssim 0.2$ Mm). When $\hat{k}_z = \hat{k}_x = b_z = -b_y = 1/\sqrt{2}$ [dotted curves in Fig. 2(a)–(b)] the growth rate is smaller than the previous case. This is because in this case the instability is not only due to the Hall diffusion but is also assisted by the ambipolar diffusion through directional dissipation of waves. Therefore, the growth rate is always smaller when both Hall and ambipolar diffusion are present in the medium. With the decreasing vertical field [$b_z = 0.1$, dash-dot curves in Fig. 2(a)–(b)] the maximum growth rate decreases further owing to smaller g and s .

The most unstable wavenumber is

$$\tilde{k}_0^2 = \frac{\tilde{\sigma}_0^2}{\left(\sqrt{\mu^2 \tilde{\eta}_H^2 + \tilde{\eta}_P \tilde{\eta}_T}\right) \tilde{\sigma}_0 - \mu^2}. \quad (45)$$

It is clear from preceding equation that when

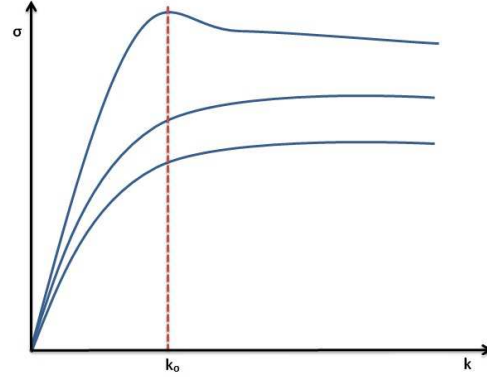


Figure 3. Above cartoon depicts growth rate against wavenumber.

$$g \tilde{\eta}_A + s \tilde{\eta}_H > 2 + \frac{\tilde{\eta}_P + \tilde{\eta}_T}{\sqrt{\mu^2 \tilde{\eta}_H^2 + \tilde{\eta}_P \tilde{\eta}_T}}, \quad (46)$$

maximum growth rate occurs at finite k_0 [see Fig. (3)]. In the opposite limit k_0 becomes imaginary implying that maximum growth rate occurs at infinity. For parameters of network-internetwork magnetic elements, with shear gradient $v'_0 \sim 10^{-2} \text{ s}^{-1}$ and $v_A \sim 10^5 \text{ km s}^{-1}$, k_0 is imaginary [corresponding to two similar curves in Fig. (3)].

4 LIMITING CASES OF THE DISPERSION RELATION

The magnetic field drift in the partially ionized plasma opens up new pathways through which the free shear energy of the fluid can be transferred to the waves (PW12a). To see this, we first note that since $\tilde{\sigma} \sim 1$, three terms in Eq. (19) are ~ 1 , \tilde{k}^2 , $\tilde{k}^2 \tilde{\eta}$ and thus, one of the following three scenarios may prevail in a diffusive medium.

A. Ideal MHD: In this limit $\tilde{k}^2 \sim 1 \gg \tilde{k}^2 \tilde{\eta}$, i.e. $\tilde{\eta} \ll 1$ and last term in Eq. (19) can be neglected. However, as has been shown in PW12a, this limit is applicable to the long wavelength fluctuations $\gtrsim 10^3 \text{ km}$ and therefore, is not relevant to the present analysis.

B. Cyclotron limit: In this case $\tilde{k}^2 \tilde{\eta} \sim \tilde{k}^2 \gg 1$. This is the low frequency limit and first term in Eq. (19) can be neglected. The low frequency, short wavelength dressed ion-cyclotron wave with frequency $\omega_C = \mu \omega_H$ is the normal mode of the system (Pandey & Wardle 2006, 2008).

Assuming $|v'_0| \sim 0.01 \text{ s}^{-1}$ and $v_A \sim 5 \times 10^5 \text{ km s}^{-1}$ we get $\tilde{\eta} \equiv \eta |v'_0|/v_A^2 \sim 10^{-2} - 10^{-4} \ll 1$ and thus it was inferred (PW12a) that the cyclotron limit is not valid in the photosphere–chromosphere. However, at an increased shear frequency $|v'_0| \lesssim 1 \text{ s}^{-1}$ we get $\tilde{\eta} \equiv \eta |v'_0|/v_A^2 \lesssim 1$ and this limit becomes important. Since recent numerical simulation with 10 – 20 km resolution (Cheung & Cameron 2012) can be easily scaled to 2 km which for typical $v_0 \sim 2 \text{ km s}^{-1}$ gives $|v'_0| \sim 1 \text{ s}^{-1}$, we conclude that the proper analysis of the cyclotron limit will provide important insight to the ongoing numerical simulations of the photosphere–chromosphere.

Taking $k \rightarrow \infty$, and thus setting $a(\sigma) = 0$ in Eq. (26) or, neglecting first matrix in Eq. (19), we get following dispersion relation

$$(\mu^2 \tilde{\eta}_H^2 + \tilde{\eta}_P \tilde{\eta}_T) \tilde{\sigma}^2 + \mu^2 (\tilde{\eta}_P + \tilde{\eta}_T) \tilde{\sigma} = \mu^2 (\gamma - \mu^2). \quad (47)$$

Positive σ requires $\gamma > \mu^2$ since coefficients on the left hand side of preceding equation are positive. Thus the stability criterion in the cyclotron limit is identical to general stability criterion, Eq. (33). This is not surprising since above dispersion relation is short wavelength limit of the general case.

The growth rate of the instability becomes

$$\tilde{\sigma} = \frac{\mu^2}{2(\tilde{\eta}_P \tilde{\eta}_T + \mu^2 \tilde{\eta}_H^2)} \left[-(\tilde{\eta}_P + \tilde{\eta}_T) + \sqrt{\Delta} \right], \quad (48)$$

where

$$\Delta = (\tilde{\eta}_P - \tilde{\eta}_T)^2 + 4\tilde{\eta}_H^2(\gamma - \mu^2) + 4\left(\frac{\gamma \tilde{\eta}_P \tilde{\eta}_T}{\mu^2}\right). \quad (49)$$

Above equation acquire particularly simple form in purely Hall or ambipolar limits. For example in the Hall diffusion dominated regime, from Eq. (48) we get

$$\sigma = \left[-v'_0 \frac{s}{\eta_H} - \mu^2 \frac{v_A^2}{\eta_H^2} \right]^{1/2} v_A, \quad (50)$$

which in $\mu < 1$ limit becomes

$$\sigma \approx [-v'_0 s \omega_H]^{1/2}. \quad (51)$$

Thus the growth rate of the dressed ion-cyclotron wave approximately equals the geometric mean of the shear and Hall frequencies and attains maximum value only for positive helicity $s = 1$.

In purely ambipolar diffusion dominated case setting $\eta_O = \eta_H = 0$, we get

$$\sigma = \frac{v_A^2}{2\eta_A} \left[-(1 + \mu^2) + \sqrt{(1 - \mu^2)^2 - \frac{4g v'_0 \eta_A}{v_A^2}} \right]. \quad (52)$$

We see from Eq. (52) that when $g = 0$, ambipolar diffusion causes only damping. As noted in the previous section, it is only when topological factor g is non-zero that anisotropic ambipolar diffusion can drive shear flow instability.

C. Highly diffusive limit : In this limit $\tilde{k}^2 \tilde{\eta} \sim 1 \gg \tilde{k}^2$, i.e. $\tilde{\eta} \gg 1$ and $\tilde{k}^2 \ll 1$. Only the first and last term in Eq. (19) are retained. For typical values of η [Table (2)], this limit gives $\lambda \lesssim 6$ km which fits within a pressure scale height. Therefore, as noted in our previous work (PW12a), highly diffusive limit is applicable to the photosphere-chromosphere.

The dispersion relation in this limit becomes

$$(\tilde{\eta}_P + \tilde{\eta}_T) \tilde{\sigma} \tilde{k}^2 + \tilde{\sigma}^2 = \tilde{k}^2 \left[\gamma - \tilde{k}^2 (\tilde{\eta}_P \tilde{\eta}_T + \mu^2 \tilde{\eta}_H^2) \right], \quad (53)$$

from where we see that for positive σ left hand side is positive. Thus right hand side must be positive. Thus we arrive at following general stability criterion

$$-v'_0 (g \eta_A + s \eta_H) > \tilde{k}^2 (\tilde{\eta}_P \tilde{\eta}_T + \mu^2 \tilde{\eta}_H^2). \quad (54)$$

In the absence of Hall diffusion, above criterion becomes

$$-v'_0 g \eta_A > \tilde{k}^2 \tilde{\eta}_P \tilde{\eta}_T. \quad (55)$$

As right hand side in the above equation is positive, the stability criterion implies that in the presence of favourable shear flow gradient ($-v'_0 > 0$) ambipolar diffusion will drive the instability only if $g > 0$. Positive topological factor g guarantees that the ambipolar diffusion will assist the shear flow in destabilising the waves.

When ambipolar diffusion is negligible, Hall diffusion can as well drive shear instability provided

$$-v'_0 s \eta_H > \tilde{k}^2 (\tilde{\eta}_O^2 + \mu^2 \tilde{\eta}_H^2). \quad (56)$$

Above criterion is similar to Eq. (24) of PW12a. Note that in PW12a, $s = 1$ as both the field and the wavevector is vertical whereas here we are dealing with the general field topology ($s \neq 1$).

The instability in the Hall-ambipolar diffusion dominated regime will grow at the maximum rate

$$\tilde{\sigma}_0 = \gamma \frac{(\tilde{\eta}_P + \tilde{\eta}_T) - 2\sqrt{\tilde{\eta}_P \tilde{\eta}_T + \mu^2 \tilde{\eta}_H^2}}{(\tilde{\eta}_P - \tilde{\eta}_T)^2 - 4\mu^2 \tilde{\eta}_H^2}, \quad (57)$$

which for purely Hall ($\eta_A = \eta_O = 0$) case reduces to Eq. (44). In the absence of Hall diffusion the maximum growth rate becomes

$$\tilde{\sigma}_0 = \frac{g \tilde{\eta}_A}{(\sqrt{\tilde{\eta}_P} + \sqrt{\tilde{\eta}_T})^2}. \quad (58)$$

When $\tilde{\eta}_O = 0$ above equation reduces to Eq. (43).

Most unstable wavelength in the highly diffusive limit becomes

$$\tilde{k}_0^2 = \frac{2\tilde{\sigma}_0^2}{[\alpha (g \tilde{\eta}_A + s \tilde{\eta}_H) - (\tilde{\eta}_P + \tilde{\eta}_T) \tilde{\sigma}_0]}. \quad (59)$$

For purely Hall case and ($\alpha = 1$) preceding acquires particularly simple form

$$\tilde{k}_0 = \sqrt{\frac{1}{2b_z \tilde{\eta}_H}}. \quad (60)$$

In purely ambipolar regime \tilde{k}_0 becomes,

$$\tilde{k}_0 = \frac{1}{(1 + \mu)} \sqrt{\frac{g}{\mu \tilde{\eta}_A}}, \quad (61)$$

from where it is clear that the most unstable wavenumber is nonzero only when the topological parameter g is nonzero. This is not surprising given that very existence of the ambipolar diffusion driven shear instability depends on the field geometry and obliqueness of the wave vector.

5 DISCUSSION

The solar photosphere is threaded by kG field concentrated in the vertical flux tubes (radius $\sim 100 - 200$ km) at intergranular boundaries (Hasan 2009). Although less frequently ($\lesssim 40\%$), field of similar strength have also been observed in the quiet solar internetwork region (Almeida et al. 2010). Outside kG patches, internetwork field is much weaker (~ 100 G). The flux tube is often modelled as non-rotating cylindrical tubes with the plasma and the magnetic pressure balance providing required stability. In the present work we have approximated flux tubes by a planer sheet where x and y coordinate locally correspond to the radial and azimuthal directions locally.

Although the chromosphere has limited extension in comparison to the corona, its net radiative loss $\sim 10^7 \text{ erg cm}^{-3} \text{ s}^{-1}$ is 10 times more than the corona. Further, except for the flares, most solar atmospheric heating occurs in the chromosphere (Aschwanden 2001; Goodman 2001). A strong correlation between core emission of calcium K and H resonance lines and quite sun magnetic field (Schrijver et

al. 1989) suggest that the origin of chromospheric heating ($\sim 10^7 \text{ ergs cm}^{-2} \text{ s}^{-1}$) is magnetic in nature. The magnetic diffusion driven shear instability proposed in the present work can provide a viable mechanism to explain the excess chromospheric heating since crucial ingredients required to excite this instability namely shear flow and magnetic field is always present in the network–internetwork region. The attractive feature of this fast growing diffusive shear instability is that all wavelengths of fluctuations are likely to be excited as there is no cut-off wavelength. Thus, as we see from Fig. (2), network field below 1 Mm is likely to be destabilised by this instability. In the internetwork elements, this instability may operate in the entire photosphere–chromosphere.

Only uncertainty involved is the lack of information about the scale of shear flow gradient which can not be resolved by current observations. However, small whirlpools with size similar to terrestrial hurricanes [$\lesssim 0.5 \text{ Mm}$ with typical lifetime $\sim 5 \text{ min.}$ on the solar surface Bonet et al. (2008)] suggest the presence of such flows. Long lasting large scale vortices at supergranular junctions with typical lifetime $\sim 1 - 2 \text{ h}$ with enhanced CaII emission have also been observed (Attie et al. 2009). The swirl motion in the chromosphere has been recently detected by Wedemeyer-Böhm & Voort (2009). Clearly, observations suggest ubiquitous presence of flow gradients in the photospheric-chromospheric plasma. Past numerical simulations also indicated the presence of vortex flows in intergranular lanes (Zirker 1993; Stein & Nordlund 1998). The typical vorticity of a vortex is $\sim 6 \times 10^{-3} \text{ s}^{-1}$ which corresponds to rotation period $\sim 35 \text{ minutes}$ (Bonet et al. 2010). Thus it would appear that Hall instability does not have time to develop since the growth rate ($|v'_0|/2 = 3 \times 10^{-3} \text{ s}^{-1}$) is very small. However, above vorticity value is limited by the upper limit in the vorticity resolution [$\sim 4 \times 10^{-2} \text{ s}^{-1}$, Bonet et al. (2010)]. The numerical simulation gives much higher vorticity value ($\sim 0.1 - 0.2 \text{ s}^{-1}$) in the photosphere-lower chromosphere (Fig. 31, Stein & Nordlund (1998)). The growth rate corresponding to $|v'_0| = 0.2 \text{ s}^{-1}$ is one minute.

For almost magnetosonic waves ($\hat{k}_z \rightarrow 0$), maximum growth rate of the Hall diffusion driven shear instability may become quite small. The maximum growth rate in the ambipolar diffusion dominated middle and upper chromosphere will be only one fifth of the Hall diffusion dominated case for the maximum $g = 0.25$ and $\mu = 0.5$. Therefore, vortex motions with typical lifetime $\gtrsim 15 \text{ min.}$ will be susceptible to the ambipolar diffusion driven shear instability. Since, vortex motions of various spatial and temporal scales are observed, it is likely that non-ideal MHD effects will play important role in exciting low frequency turbulence in the medium.

The *non-ideal* MHD description of the photosphere-chromosphere provides several pathways through which shear energy can be channelled to the waves by magnetic field. For example in excessively diffusive limit when $\delta \mathbf{v}/v \ll \delta \mathbf{B}/B$, diffusion in tandem with the shear flow can destabilise the network-internetwork field. For purely vertical field and vertical wavevector this limit has been discussed in detail in PW12a. In order to compare with PW12a, we briefly describe the effect of the field topology and wave orientation in the highly diffusive limit. Comparing Figs. 2 and 4 we conclude that the maximum growth rate is similar in both cases. When $b_z = \hat{k}_z = 1$, instability grows at maxi-

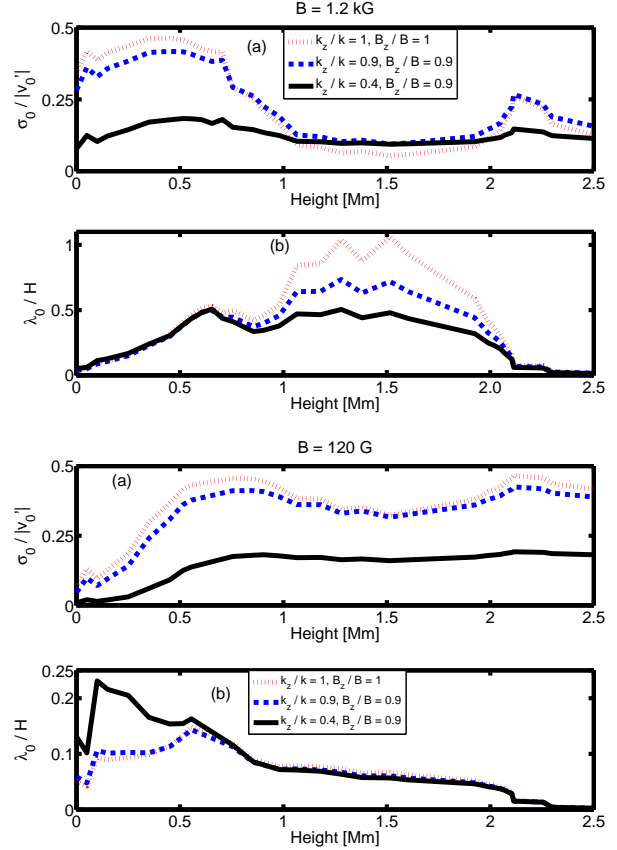


Figure 4. The growth rate and most unstable wavelength is shown for 1.2 kG [Fig. 4(a)] and 120 G [Fig. 4(b)] fields. Following parameters have been used in the above figure: $\hat{k}_z = 1, b_z = 1$ (bold line), $\hat{k}_z = b_z = 0.9$ (dashed line) and $\hat{k}_z = 0.4, b_z = 0.9$ (dotted line).

um rate whereas with decreasing \hat{k}_z or b_z the growth rate diminishes.

In Fig. 4(b) we plot most unstable wavelength against height for same parameters as in Fig. 4(a). The wavelength is normalized against scale height calculated self-consistently using model C, VAL81. For both kG and weaker field λ_0 fits well within a scale height and thus the instability will grow at maximum rate in the entire photosphere–chromosphere. However, it is only in the photosphere and lower chromosphere ($\lesssim 1 \text{ Mm}$) where the instability will grow at maximum rate for a kG field. In the middle and upper chromosphere the growth rate tapers off and becomes one eighth of shear frequency. Therefore, in the strong field region, diffusive instability will be efficient in destabilizing magnetic element in the photosphere and lower chromosphere. When the field is weak ($\sim 100 \text{ G}$), the instability can operate in the entire photosphere-chromosphere at maximum rate.

How does nonlinear saturated state of diffusive instability will look like? The answer to this can be given only by numerical simulations. However, if the nonlinear results of the protoplanetary discs and star forming regions are any guide then this instability should be quite efficient in exciting the low frequency turbulence and heating of the plasma. In fact interplay between the vortex flow and magnetic dif-

fusion could be responsible for entire energy budget of the solar atmosphere.

The energetic events such as hard x-ray emissions ($\sim 10^{26} \text{ erg s}^{-1}$) are believed to be due to the presence of energetic electrons with energies above ($\sim 20 \text{ keV}$) in the solar flares. One of the plausible scenarios for the electron acceleration to such high energies requires turbulent medium. The stochastic acceleration of the electron by the turbulent wave spectrum produces high energy spectrum (Fletcher & Hudson 2008). Since magnetic diffusion could be important agent in driving the diffusive shear instability, this could easily lead to the low frequency turbulence in the medium. However, further work is needed in this direction to support this hypothesis.

6 SUMMARY

The granular motion is responsible for the generation of low frequency Alfvén wave in the predominantly neutral photosphere. Unlike high-frequency MHD counterpart which undergo damping (Vranjes et al. 2007, 2008), low frequency Alfvén wave generally propagate undamped in the medium. In the presence of shear flow gradient, the solar photosphere-chromosphere region can become unstable due to non-ideal MHD effects. Depending on the shear scale, such instability can be excited at all wavelengths. The presence of favourable magnetic field topology will facilitate the transfer of shear energy to the magnetic fluctuations. The instability in the solar atmosphere is due to the presence of two unrelated physical processes (a) *nonideal* MHD effects and, (b) shear flow.

The following are the itemized summary of the present work.

1. The magnetic diffusion in the presence of shear flow makes solar atmosphere susceptible to diffusive shear instability. The instability depends on the sign of the shear gradient and on the local magnetic field topology.
2. Purely vertical magnetic field and vertical wavevector along with the shear flow is fundamental to this Hall diffusion driven instability.
3. Only when field has non-vertical component and waves are propagating obliquely, both Hall and ambipolar diffusion together can assist this instability.
4. The maximum growth rate of the instability which is proportional to the absolute value of the shear gradient occurs when both the field and the wavevector is vertical.
5. The e-folding time of the magnetic diffusion driven shear instability is very short ($\sim 20 \text{ s}$ for $v'_0 = 0.1 \text{ s}^{-1}$) suggesting that the flux tubes are likely to be susceptible to this fast growing instability.

ACKNOWLEDGMENTS

The financial support of Australian Research Council through grants DP0881066 and DP120101792 is gratefully acknowledged. This research has made use of NASA's Astrophysics Data System.

REFERENCES

- Almeida J. S., Bonet, J. A., Viticchié, B. & Del Moro, D., 2010, *ApJ*, 715, L26
- Almeida J. S., González, M. M., 2011, *astro-ph/arXiv:1105.0387v1*
- Arber T. D., Haynes, M. & Leake J. E., 2007, *ApJ*, 666, 541
- Aschwanden, M., 2009, *Physics of the Solar Corona*, (UK: Springer-Praxis)
- Aschwanden, M. J. 2001, *ApJ*, 560, 1035
- Attie R., Innes D. E. & Potts, H. E., 2009, *A&A*, 493, L13
- Balbus S. A. & Hawley J. F., 1998, *Review of Mod. Phys.*, 70, 1 (BH98)
- Balbus S. A. & Terquem C., 2001, *ApJ*, 552, 235
- Balmaceda, L., Vargas Domínguez, S., Palacios, J., Cabello, I., & Domingo, V. 2010, *A&A*, 513, L6
- Bonet, J. A., Márquez, I., Almeida, J. S., Cabello, I. & Domingo, V., 2008, *ApJ*, 687, L131
- Bonet, J. A., Márquez, I., Almeida, J. S., Palacios, J., Pillet, V. M., Solanki, S. K. et al., 2010, *ApJ*, 723, L139
- Braginskii, S. I. 1965, *Review of Plasma Physics* (vol 2) ed. Leontovich, M. A., 1965, 205 (New York: Consultants Bureau)
- Chandrasekhar, S. 1961, *Hydrodynamic & Hydromagnetic Stability*, (Cambridge: Cambridge University Press)
- Cheung, C. M. M. & Cameron R. H., *arXiv:1202.1937*
- Cowling, T. G. 1957, *Magnetohydrodynamics*, (Bristol: Adam Hilger)
- Desch, S. 2004, *ApJ*, 608, 509
- de Wijn A. G., Stenflo, J. O., Solanki, S. K. & Tsuneta S., 2009, *Space Sci. Rev.*, 144, 275
- Erdelyi R. & James S. P., 2004, *A&A*, 427, 1055
- Fletcher L. & Hudson H. S., 2004, *ApJ*, 675, 1645
- Fontana, P. R., 1961, *Phys. Rev*, 123, 1865
- Foullon C., Verwichte, E., Nakariakov, V. M., Nykri, K. & Farrugia C. J., 2011, *ApJ*, 729, L8
- Glassgold, A. E., Krstić, P. S. & Schultz, D. R., 2005, *ApJ*, 621, 808
- Goedbloed, H. & Poedts S. 2004, *Principles of Magnetohydrodynamics with Applications to laboratory and Astrophysical Plasmas*, (London: Cambridge)
- Goodman, M. L. 2001, *Sp.Sci.Rev*, 95, 79
- Goodman, M. L. 2004, *A&A*, 416, 1159
- Goodman, M. L. 2011, *ApJ*, 735, 45
- Hasan, S. 2009, in N. Goplaswamy & D. F. Webb (eds.) *Universal Heliophysical Processes*, IAU Symp. 257, 121
- Hasan, S. & Kalkofen, W. 1999, *ApJ*, 519, 899
- Khodachenko, M. L., Arber, T. D., Rucker, H. O. & Hanslmeier, A., 2004, *A&A*, 279, 389.
- Khomenko E. & Collados M., 2012, *ApJ*, 747, 87
- Karpen, J. T., Antiochos, S. K., Dahlburg, R. B. & Spicer D. S., 1993, *ApJ*, 403, 769
- Kolesnikov, F., Bunte, M., Schmitt, & Schussler M., 2004, *A&A*, 420, 737
- Krstić, P. S. & Schultz, D. R., 2009, *Phys. Plasmas*, 16, 053503.
- Kudoh, T. and Shibata, K.: 1997, in A. Wilson (ed) *Proc. of the Fifth SOHO Workshop*, ESA SP-404, pp. 477
- Kunz, M. W. & Balbus S. A., 2004, *MNRAS*, 348, 355 (KB04)
- Kunz, M. W., 2008, *MNRAS*, 385, 1494 (K08)

Leake J. E. & Arber T. D., 2006, *A&A*, 450, 805
 Leake J. E., Arber T. D. & Khodachenko M. L., 2005, *A&A*, 442, 1091
 Lites B. W., Kubo M., Socas-Navarro H. et al., 2008, *ApJ*, 672, 1237
 Longmire C. L. & Rosenbluth M. N., 1956, *Phys. Rev.*, 103, 507
 Martinez P. V., Lites, B. W. & Skumanich A., 1997, *ApJ*, 474, 810
 Mestel L. & Spitzer L., 1956, *MNRAS*, 116, 504 (MS56)
 Moll R., Cameron, R. H. & Schüssler M., 2011, *A&A*, 533, A126
 Muthsam, H. J., Kupka, F., Löw-Baselli, B., Obertscheider, C., Langer, M. & Lenz, P. 2010, *New Astron.*, 15, 46
 Nordlund, A., Stein, R. F., & Asplund, M. 2009, *Living Rev. Sol. Phys.*, 6, 2
 Ofman, L. & Thompson, B. J., 2011, *ApJ*, 734, L11
 Pandey B. P. & Wardle, M., 2006, *astroph/0608008*
 Pandey B. P. & Wardle, M., 2008, *MNRAS*, 385, 2269
 Pandey B. P., Vranjes, J. & Krishan, V., 2008, *MNRAS*, 386, 1635
 Pandey B. P. & Wardle, M., 2012a, *MNRAS*(in press), *astroph/arXiv:1108.3169v1*,
 Pandey B. P. & Wardle, M., 2012b, *MNRAS*, 423, 222
 Parker, E. N., 1979, *Cosmic Magnetic Fields*, (Oxford: Clarendon Press)
 Parhi,S., Pandey, B. P., Goossens,M., Lakhina G. S., de Bruyne P.,1997, *Ap&SS*, 250, 147
 Parhi,S., Pandey, B. P., Lakhina G. S, Goossens,M. & de Bruyne P. 1997, *AdSpR*, 19, 1891
 Parhi,S., Pandey, B. P., Goossens,M. & Lakhina, G. S. 1998, *IAU*, 185, 457
 Petrovic,D., Vranjes,J., Poedts,S., 2007, *A&A*, 461, 277
 Priest, E. R. 1987, *Solar Magnetohydrodynamics*, (Dordrecht: D. Reidel)
 Schüssler, M. 1984, *A&A*, 140, 453
 Schrijver, C. J., Cote, J., Zwaan C. & Saar, S. H., 1989, *ApJ*, 337, 964
 Schüssler M., 1984, *A&A*, 140, 453
 Spiegel, E. A., & Veronis, G. 1960, *ApJ*, 131, 442
 Shelyag, S., Keys, P., Mathioudakis M. & Keenan, F. P., 2011, *A&A*, 526, A5
 Solanki, S. K., Keller, C., & Stenflo, J. O. 1987, *A&A*, 188, 183
 Soler, R., Terradas, J., Oliver, R., Ballester, J. L. & Goossens, M. 2010, *ApJ*, 712, 875
 Stein, R. F., & Nordlund, A. 1998, *ApJ*, 499, 914
 Stenflo, J. O., Solanki, S. K., & Harvey, J. W. 1987, *A&A*, 171, 305
 Steiner, O. & Rezaei, R., 2012, *arXiv:1202.4040v1*
 Sykora, J. M., De Pontieu, B. & Hansteen, V., 2012, *ApJ*, 753, DOI:10.1088/0004-637X/753/2/161
 Vernazza J. E., Avrett E. H. & Loser, R., 1981, *ApJS*, 45, 635
 Vranjes, J., Poedts, S. & Pandey, B. P., 2007, *Phys. Rev. Lett.*, 98, 049501
 Vranjes, J., Poedts, S., Pandey, B. P. & De Pontieu, B. 2008, *A&A*, 478, 553
 Wardle M., 1999, *MNRAS*, 307, 849
 Wardle M., 2007, *Astroph.Sp.Sci.*, 311, 35
 Wardle M. & Salmeron R., 2011, (*astroph/arxiv:1103.3562v1*)

Wedemeyer-Böhm S. & Voort, L. V., 2009, *A&A*, 507, L9
 Zaqarashvili, T. V., Diaz, A. J., Oliver, R. & Ballester, J. L. 2010, *A&A*, 516, A84.
 Zirker J. B., 1993, *Sol. Phys.*, 147, 47

APPENDIX A:

Often, ion-neutral collision frequency is calculated by assuming collision cross-section $\sigma = 10^{-15} \text{ cm}^2$ (Khodachenko et al 2004). This cross-section is even smaller than $H^+ + H$ collision becomes clear, if we recall that, proton-neutral hydrogen cross-section is well described by the following power law at low energies (Glassgold et al. 2005)

$$\sigma(E) = \sigma(E_1) \left(\frac{E}{E_1} \right)^p \quad (\text{A1})$$

where $E_1 = 0.01 \text{ eV}$ and $\sigma(E_1) = 1.65 \times 10^{-14} \text{ cm}^2$ (590 amu). In solar atmosphere, $E > E_1$ and $p = -1/8$. For Model C, VAL81, $\sigma \approx 10^{-14} \text{ cm}^2$. Thus, if we assume that ion-neutral collision is solely due to the ionised and neutral hydrogen, the ion-neutral collision frequency will be an order of magnitude higher than when $\sigma \approx 10^{-15} \text{ cm}^2$.

However, lower solar atmosphere is populated mainly by the metallic ions and neutral Hydrogen and thus, the collision cross-section given by Eq. (A1) underestimates the collision frequency. Further, the quantum effects could also become important. Thus, it is important to find an analytical expression for the momentum transfer cross-section. At low energies ($\leq 10^4 \text{ K}$), the elastic cross-section can be well approximated by Massey-Mohr cross section (Krstić & Schultz 2009)

$$\sigma_{MM} = 5 \times 10^{11} \left(\frac{C_6}{v} \right)^{2/5} \text{ cm}^2. \quad (\text{A2})$$

Here C_6 is the dipole-dipole coefficient in the interaction potential which can be expressed in terms of polarisabilities α and ionisation energies E of two interacting atoms (Fontana 1961)

$$C_6 = 1.5 \alpha_1 \alpha_2 \frac{E_1 E_2}{E_1 + E_2}. \quad (\text{A3})$$

The value of C_6 varies between $1.26 \times 10^{-60} \text{ erg-cm}^3$ for He to $2200 \times 10^{-60} \text{ erg-cm}^3$ for Cs (Fontana 1961). Therefore, we assume $C_6 = 100 \times 10^{-60} \text{ erg-cm}^3$. Since the cross-section is proportional to $C_6^{0.4}$, the assumed value of C_6 will not significantly affect the collision cross-section. The collision rate is

$$< \sigma_{MM} v >_{in} = 3.15 \times 10^{12} v^{3/5} \text{ cm}^3 \text{ s}^{-1} \quad (\text{A4})$$

which can also be written as

$$< \sigma_{MM} v >_{in} = 7.91 \times 10^{-10} T^{0.3} \text{ cm}^3 \text{ s}^{-1}. \quad (\text{A5})$$

Here we have assumed $v = \sqrt{k_B T / m_i}$. The resulting value of ν_{in} is an order of magnitude smaller than has been assumed by Vranjes et al. (2008) owing to their arbitrary mass-scaling of the cross-section.

The electron-neutral collision rate is assumed as

$$< \sigma v >_{en} = 10^{-15} \left(\frac{128 k_B T}{9 \pi m_e} \right) \equiv 8.28 \times 10^{-10} \sqrt{T} \text{ cm}^3 \text{ s}^{-1}. \quad (\text{A6})$$

For similar reasons, the electron-neutral collision frequency in the present case is an order of magnitude smaller than given by Vranjes et al. (2008); Pandey et al. (2008).